Acoustic Wave Resonator-Based Bandpass Filters With Continuously Tunable Fractional Bandwidth

Mohammed R. A. Nasser, *Graduate Student Member, IEEE*, and Dimitra Psychogiou, *Senior Member, IEEE*

***Abstract*—A new class of acoustic-wave resonator-based bandpass filters (BPFs) with continuously tunable fractional bandwidth (FBW) are presented. They are based on cascaded multi-resonant stages of hybridly-integrated surface acoustic wave (SAW) resonators with lumped element (LE) components. Each stage comprises one SAW resonator and one or more LE resonators that contribute to the overall transfer function to one pole and two transmission zeros (TZs). As such highly-selective quasi-elliptic transfer functions with *N* poles, 2*N* TZs and enhanced FBW can be created for two series and *N-2* parallel stages. It is shown that by reconfiguring the resonant frequency of the LE resonators, continuously-tunable FBWs can be obtained. The operating principles of the multi-stage concept are demonstrated through design examples of multi-stage prototypes. The concept has been validated at 916.6 MHz through a four-pole/eight-TZ BPF with tunable BW between 0.63–1.32 MHz (i.e., FBW = 0.57 − 1.32k_t^2), minimum in-band insertion loss (IL) 3.9-2.3 dB (Q_{eff} = 7700-6000) and out-of-band isolation > 27 dB.**

***Index Terms*—Acoustic wave resonator (AWR), high quality factor (Q), tunable bandpass filter (BPF), k_t^2-enhancement.**

I. Introduction

ADAPTIVE RF front-ends are increasingly desired in modern communication systems due to the unprecedented growth and diversity of wireless communication standards [1]. Bandpass filters (BPFs) with electronically reconfigurable transfer functions are highly-desirable in these systems to enhance existing capabilities, and miniaturize their size [2]. The majority of the tunable BPFs that have been presented to date are large in size and are based on low-quality factor (Q) (around 50-150 for lumped-element (LE) and microstrip-type configurations [3], [4], and 300-800 for coaxial-resonator-based components [5]) resonators. These also exhibit high levels of in-band insertion loss (IL) between 3-10 dB [4], [6]. In yet another approach, RF filters using surface acoustic wave (SAW) and bulk acoustic wave (BAW) resonators exhibit high Q (order of a thousand) and chip-scale size. However, they are limited by static transfer function and narrow fractional bandwidth (FBW) around 0.4-0.8k_t^2, where k_t^2 is the electromechanical coupling coefficient [7]. Thus, recent research efforts are focused on enhancing the FBW and on enabling transfer function reconfigurability.

Alternative SAW-based tuning concepts have been explored to date. However, most of them facilitate discrete RF tuning. For example, in [12], [13], a ferroelectric material is used within a thin-film bulk acoustic resonator (FBAR) resonator to turn its resonance ON or OFF in the presence or absence of DC biasing. This concept has been exploited for the realization of intrinsically-switchable filter banks and RF filters with tunable FBW, however it relies on a fairly complicated manufacturing process and is only suitable for discrete tuning. Switchable SAW-based dual-band BPFs filters have also been proposed in [14]. They are based on the co-integration of SAW resonators with vanadium oxide (VO_2)-based switches. However, they suffer from high IL (> 10 dB).

In terms of FBW enhancement, acoustic-wave resonators (AWRs) using new types of thin-film materials (e.g., the ScAlN technology in [8], [9]) or alternative types of resonating modes (e.g., SH mode SAW resonators in [10], [11]) have been demonstrated, however they suffer from in-band ripples and spur resonances. In yet another approach, FBW widening is achieved through hybrid integration of AWRs and electromagnetic (EM) components. In [15], [16], AWRs are combined with microstrip transmission lines. Such an approach occupies large size due to the use of distributed elements.

In yet another configuration, AWRs are combined with lumped-element (LE) components in acoustic-wave-lumped-element resonator (AWLR) architectures. In this manner, FBWs wider than the 0.4-0.8k_t^2 limit can be obtained while preserving the high Q of AWRs and exhibiting small size. Moreover, they enable transfer function reconfigurability. Notable demonstrations include filters with: i) reconfigurable bandpass-to-bandstop response [17] ii) reconfigurable all-pass-to-bandstop response [18] and iii) tunable FBW and out-of-band characteristics [19], [20]. However, most of these concepts aren't electronically-reconfigurable and are tuned manually with trimmer capacitors.

Considering the aforementioned limitations, this brief reports on a new class of quasi-elliptic AWLR-based BPFs with electronically-reconfigurable FBW. They are based on cascaded series- and parallel-type multi-resonant AWLR stages whose transfer function characteristics are tuned by electronically-reconfigurable varactors. As opposed to conventional AWR-based filters, it facilitates highly-selective quasi-elliptic transfer functions with enhanced (i.e., FBW> 0.4-0.8k_t^2) and continuously-tunable FBW while exhibiting high effective quality factor (Q_{eff}), and using identical AWRs.

Manuscript received 1 August 2022; revised 27 October 2022; accepted 19 November 2022. Date of publication 8 December 2022; date of current version 29 March 2023. This work was supported by the Science Foundation Ireland (SFI) under Project 20/RP/8334. This brief was recommended by Associate Editor Y. Wu. *(Corresponding author: Mohammed R. A. Nasser.)*

Mohammed R. A. Nasser is with the Advanced RF Technologies, Tyndall National Institute, Cork, T12 R5CP Ireland, and also with the School of Engineering, University College Cork, Cork, T12 K8AF Ireland (e-mail: mohammed.nasser@tyndall.ie).

Dimitra Psychogiou is with the School of Engineering, University College Cork, Cork, T12 K8AF Ireland, and also with Tyndall National Institute, Cork, T12 R5CP Ireland (e-mail: dpsychogiou@ucc.ie).

Color versions of one or more figures in this article are available at https://doi.org/10.1109/TCSII.2022.3225735.

Digital Object Identifier 10.1109/TCSII.2022.3225735

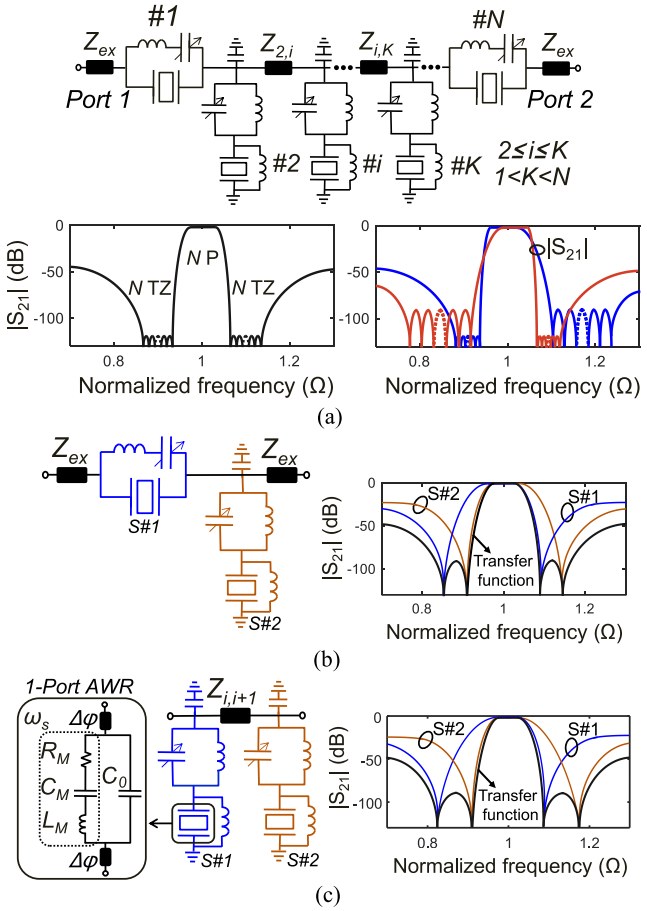

Fig. 1. Quasi-elliptic AWLR-based BPF that exhibits N poles and $2N$ TZs. (a) Generalized block diagram and example transfer functions. (b) Circuit schematic and example response of a filter comprising one series-type and one parallel-type stages. (c) Circuit schematic and example response of a filter comprising two parallel-type stages.

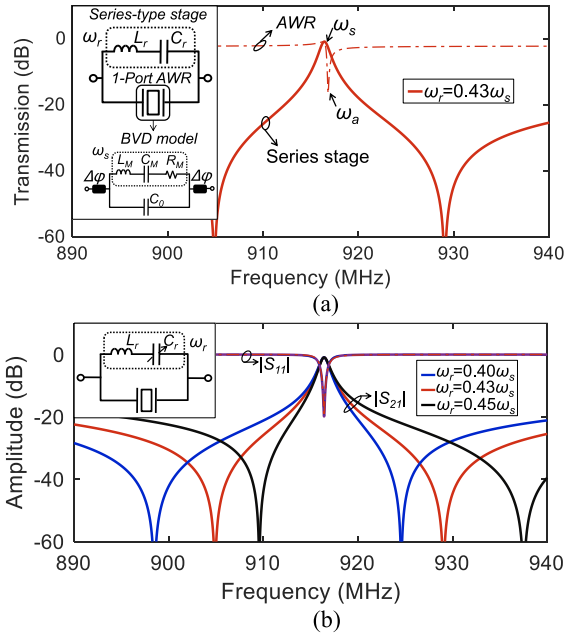

Fig. 2. (a) Simulated power transmission $|S_{21}|$ of a SAW resonator (C_M = 1.848 fF, L_M = 16.321 μH, R_M = 11.3 Ω, C_0 = 2.18 pF, $\Delta\varphi$ = 9.38°, k_t^2 = 0.12%, f_s = 916.4 MHz) and a series-type AWLR multi-resonant stage. (b) Power transmission response $|S_{21}|$ of the series-type multi-resonant stage that exhibits one pole and two TZs. The TZs can be controlled by altering ω_r.

The content of this brief is organized as follows. Section II presents the theoretical foundations of the proposed multi-stage AWLR-based BPFs concept through alternative design examples. Realistic implementation effects using lossy resonators and LEs are also discussed. The experimental validation of the concept is presented in Section III through the manufacturing and testing of a four-stage prototype. Finally, the major contributions of this brief are summarized in Section IV.

II. Theoretical Foundations

A. Multi-Stage AWLR-Based Filter Concept

The generalized block diagram of the proposed multi-stage AWLR-based BPF concept is illustrated in Fig. 1(a). It is based on the cascade of two series-type multi-resonant stages—coupled to the RF ports via impedance inverters (Z_{ex})—and $N-2$ parallel-type multi-resonant stages that are cascaded by $N-3$ impedance inverters ($Z_{2,i}-Z_{i,K}$). In this manner, highly-selective quasi-elliptic transfer functions with N poles, $2N$ TZs can be obtained. By reconfiguring the resonant characteristics of the LE resonators in each stage, the TZs can be either placed symmetrically or asymmetrically around the passband [see Fig. 1(a)] allowing to tailor the roll-off and out-of-band rejection. This is also shown in the conceptual examples of two different two-stage BPFs that either comprise of one-series-type and one parallel-type stages or two parallel-type stages as illustrated in Fig. 1(b), (c). To better illustrate the operating principles of the multi-stage AWLR BPF concept various design examples of the multi-resonant stages and their use in high-order BPFs are considered next.

B. Multi-Resonant AWLRs

The circuit details of the series-type multi-resonant AWLR stage are illustrated in Fig. 2(a). One AWR (series resonant frequency: ω_s, parallel resonant frequency: ω_a) is cascaded in parallel with a series-type LE resonator (resonant frequency $\omega_r = 1/(C_r L_r)^{1/2}$) that decouples ω_a from ω_s. In this manner, a quasi-elliptic response that has one-pole and two-TZ can be obtained [see Fig. 2(a)]. The location of the pole and TZs can be specified using (1), (2). It should be noted that the TZs can be reconfigured around the pole by altering ω_r that resonates at frequencies *0.45x* lower than ω_s as shown in Fig. 2(b).

The circuit schematic and the theoretical S-parameters of the parallel-type multi-resonant stage are depicted in Fig. 3. It is made up of an AWR that is connected in parallel with an inductor L_0 and is cascaded in series with a parallel LE resonator (resonant frequency $\omega_p = 1/(C_p L_p)^{1/2}$). The LE resonator resonates at ω_p 1.2x higher than ω_s; and together with its neighboring elements acts as an impedance inverter. In this manner, a quasi-elliptic response having one-pole and two-TZ can be created [see Fig. 3(a)] whose frequencies can be specified using (3), (4). Moreover, the resulting TZs can be tuned around the transmission pole by altering ω_p, as shown in Fig. 3(a). The parallel-type multi-resonant stage can be designed for arbitrary FBW states by appropriately adjusting the inductance ratio (L_p/L_0) as illustrated in Fig. 3(b).

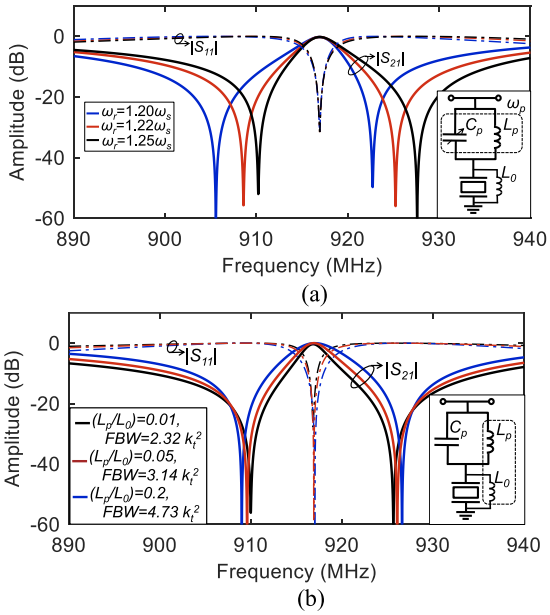

Fig. 3. Power transmission $|S_{21}|$ and reflection $|S_{11}|$ responses of the parallel-type AWLR multi-resonant stage. (a) TZs control around the pole by tuning ω_p. (b) BW control by altering (L_P/L_0).

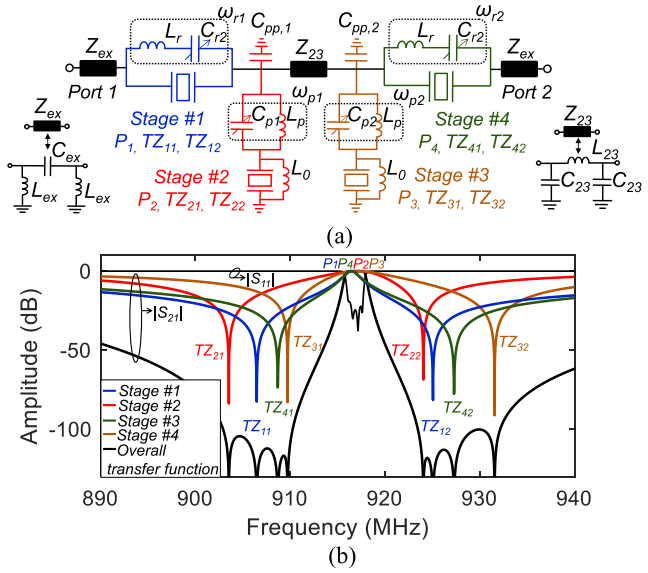

Fig. 4. (a) Circuit schematic of the quasi-elliptic four-pole/eight-TZ AWLR BPF that comprises four multi-resonant AWLR stages. (b) Theoretical power transmission $|S_{21}|$ and reflection $|S_{11}|$ of the BPF and its constituent stages (Stage #1, Stage #2, Stage #3 & Stage #4) obtained with linear circuit simulations.

C. High Order Quasi-Elliptic AWLR-Based BPFs

Considering the operating principles of the multi-resonant stages, highly-selective transfer functions can be designed. Specifically, Fig. 4, illustrates how a four-pole/eight-TZ quasi-elliptic (TZ) transfer function with enhanced FBW can be obtained by cascading two series-type (stage #1, stage #4) and two-parallel type multi-resonant stages (stage #2, stage#3). Their poles and TZs can be specified using (1)–(4), shown at the bottom of the page. The cascading of the multi-resonant stages makes the placement of the poles and the TZs in the overall BPF governed by the individual multi-resonant stages. This allows flexibility in reconfiguring the response; for example, the TZs can be reconfigured to show different roll-off rates around the passband by controlling the resonance of the LE resonators of each constituent stage as demonstrated in Fig. 5. Unlike the conventional ladder-type AWR based filter designs, the proposed configuration enables the design of passbands with arbitrary FBWs (>0.4-0.8 k_t^2) as shown in Fig. 6 where FBWs: 1-2.65k_t^2 are illustrated. They are achieved by adjusting L_p/L_0 along with C_{pp1}, C_{pp2}, Z_{23} and Z_{ex}. In these examples, inverters Z_{23} and $Z_{ex}$are replaced with their π-type LE equivalent using the following: $L = Z/\omega_{cen}$, $C = 1/(Z\omega_{cen})$ and $\omega_{cen} = 2\pi f_{cen}$, where f_{cen} is the centre frequency and Z the inverter impedance.

To evaluate the performance of the filter in the presence of lossy elements, finite Q is considered for the transfer function example in Fig. 7 where Q_M is the Q factor of the AWRs and Q_{LE} is the Q of the auxiliary lumped elements (21 total). As shown, Q_{LE} has minimal effect on the in-band IL and the passband preserves the high-Q SAW resonator characteristics. On the other hand, low Q_{LE} primarily affects the out-of-band attenuation levels. However, even with Q_{LE} as low as 62.5, the attenuation levels are higher than 60 dB.

The multi-stage AWLR-based BPF concept can be readily scaled to the realization of high order transfer functions. This

$$\omega_{\text{Pole}}^{\text{Series}} = \frac{1}{\sqrt{C_M L_M}} \tag{1}$$

$$\omega_{TZ1,2}^{\text{Series}} = \sqrt{\frac{(C_0+C_r)\omega_s^{-2} + (C_0+C_M)\omega_r^{-2} \pm \sqrt{\left((C_0+C_r)\omega_s^{-2}\right)^2 + \left((C_M+C_0)\omega_r^{-2}\right)^2 + \left(2C_rC_M - 2C_0C_M - 2C_0C_r - 2C_0^{-2}\right)\omega_s^{-2}\omega_r^{-2}}}{2C_0\omega_r^{-2}\omega_s^{-2}}} \tag{2}$$

$$\omega_{\text{Pole}}^{\text{Parallel}} = \sqrt{\frac{C_M L_0 + W_0^{-2} + \omega_s^{-2} \pm \sqrt{\omega_0^{-4} + \omega_s^{-4} + 2C_M L_0(\omega_0^{-2}+\omega_s^{-2}) - 2\omega_0^{-2}\omega_s^{-2} + C_M^2 L_0^2}}{2\omega_0^{-2}\omega_s^{-2}}} \tag{3}$$

$$\omega_{TZ1,2}^{\text{Parallel}} = \sqrt{\frac{jL_P(\omega_0^{-2} + L_0C_M + \omega_s^{-2}) + jL_0(\omega_s^{-2} + \omega_P^{-2}) \pm \sqrt{X}}{2j\omega_s^{-2}(\omega_0^{-2}L_P + \omega_P^{-2}L_0)}} \tag{4}$$

$$\begin{aligned} X = &-\left(L_P^2 + L_0^2\right)\omega_s^{-4} - 2L_0L_P\left(\omega_s^{-4} - \omega_0^{-2}\omega_s^{-2} + \omega_0^{-2}\omega_p^{-2} - \omega_s^{-2}\omega_p^{-2}\right) - 2C_ML_0L_P^2\left(\omega_s^{-2} + \omega_0^{-2}\right) - 2C_ML_PL_0^2\left(\omega_s^{-2} + \omega_p^{-2}\right) \\ &- L_P^2\left(\omega_0^{-4} - 2\omega_0^{-2}\omega_s^{-2} + C_M^2L_0^2\right) - L_0^2\left(\omega_p^{-4} - 2\omega_s^{-2}\omega_p^{-2}\right) \end{aligned} \tag{5}$$

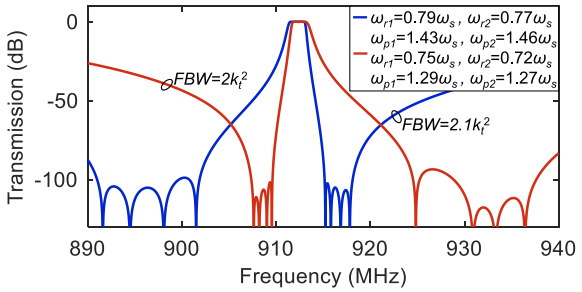

Fig. 5. Theoretical power transmission $|S_{21}|$ response of the four-stage quasi-elliptic BPF for alternative locations of TZs (by altering ω_{r1}, ω_{r2}, ω_{P1}, ω_{P2}) demonstrating the reconfigurability of the transfer function in the out-of-band.

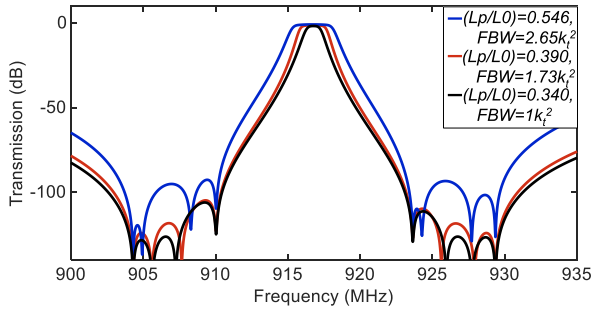

Fig. 6. Theoretical power transmission $|S_{21}|$ response of the four-stage quasi-elliptic BPF for alternative levels of FBW by altering the inductance ratio L_P/L_0 and the impedance inverter values. For the case of: i) $L_P/L_0 = 0.546$, $C_{pp1} = C_{pp2} = 0.51$ pF, $C_{p1} = 2.77$ pF, $C_{p2} = 2.69$ pF, $C_{ex} = 1.32$ pF, $L_{ex} = 17$ nH, $C_{23} = 0.63$ pF, $L_{23} = 33.2$ nH, ii) $L_P/L_0 = 0.39$, $C_{pp1} = C_{pp2} = 0.89$ pF, $C_{p1} = 2.02$ pF, $C_{p2} = 2.08$ pF, $C_{ex} = 1.94$ pF, $L_{ex} = 14.5$ nH, $C_{23} = 0.66$ pF, $L_{23} = 22.4$ nH, ii) $L_P/L_0 = 0.34$, $C_{pp1} = C_{pp2} = 0.51$ pF, $C_{p1} = 1.934$ pF, $C_{p2} = 1.888$ pF, $C_{ex} = 1.32$ pF, $L_{ex} = 17.06$ nH, $C_{23} = 0.626$ pF, $L_{23} = 29.9$ nH. (The rest of design parameters are: $L_{p1} = L_{p2} = 7.6$ nH, $L_{r1} = L_{r2} = 25$ nH, $C_{r1} = C_{r2} = 2.15$ pF).

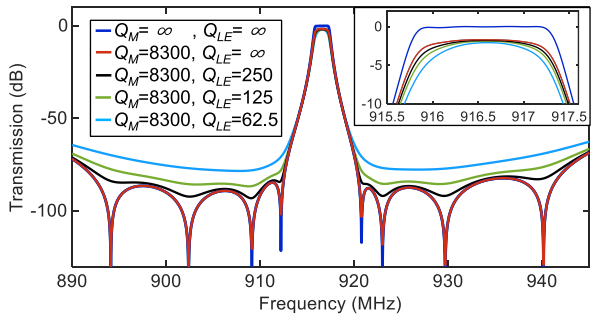

Fig. 7. Theoretical power transmission $|S_{21}|$ response of the four-stage four-pole/eight-TZ BPF as a function of Q_M and Q_{LE}.

is shown in Fig. 9 for the case of a six-stage BPF design that is comprised of two series-type stages and four parallel-type stages and exhibits six-poles and twelve-TZs.

D. Bandwidth Tuning

The bandwidth tuning concept for the devised multi-stage AWLR BPF concept is illustrated in Fig. 8 for the example case of a four-pole/eight-TZ BPF. It is performed by altering the TZs around the passband. Specifically, by decreasing ω_{r1} and ω_{r2}, (achieved by lowering $C_{r1,2}$) the TZs associated with the series stages (located on the upper edge of passband) are brought closer to the center frequency. Likewise, by increasing ω_{p1} and ω_{p2} (achieved by lowering $C_{p1,2}$), the TZs of parallel stages (located at the lower edge of passband) are brought

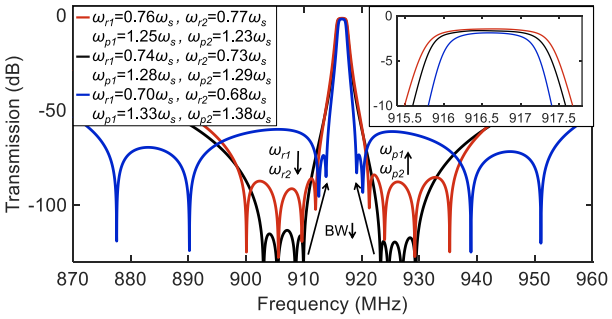

Fig. 8. Theoretical power transmission $|S_{21}|$ response of the four-stage four-pole/eight-TZ BPF. Continuous BW tuning is obtained by varying the location of the TZs.

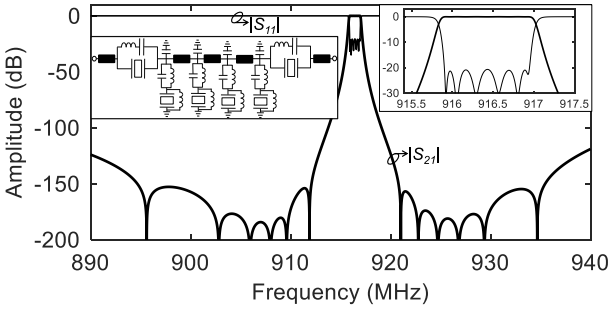

Fig. 9. Circuit schematic of the six-stage six-pole/twelve-TZ BPF alongside with its ideally-simulated S-parameters.

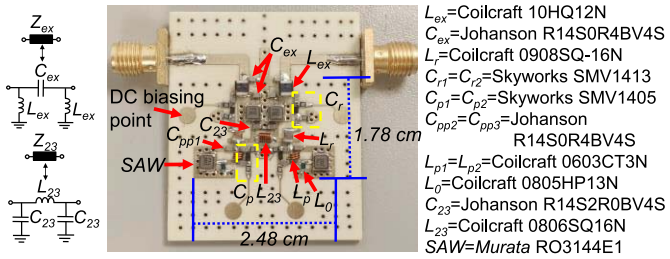

Fig. 10. Manufactured prototype of four-stage quasi-elliptic AWLR prototype.

closer to the center frequency. In this manner, the FBW can be tuned to narrower stages. As shown in Fig. 8, when tuning the FBW to narrower states, the isolation levels close to the passband decrease whereas the isolation bandwidth widens due to some of the TZs having moved to distant frequencies.

III. Experimental Validation

To validate the proposed AWLR-based quasi-elliptic BPF concept, a four-stage (N=4) BPF prototype exhibiting four-poles and eight-TZ has been designed, manufactured and tested. The prototype was implemented at 916.6 MHz using commercially-available SAW resonators from Murata Inc. and LE components from Coilcraft Inc. and Johanshon. RF tuning is performed using Skywork Varactors. The design was performed on Roger 4003C substrate (dielectric thickness H = 0.813 mm, permittivity ε_r = 3.55), using the software package Keysight ADS and following the design guidelines in Section II. RF characterization was performed by means of S-parameters using a Keysight N5244A network analyzer. The photograph of the manufactured four-stage AWLR BPF prototype is shown in Fig. 10 alongside the details of the utilized SMD components. In Fig. 11, the RF-measured response of

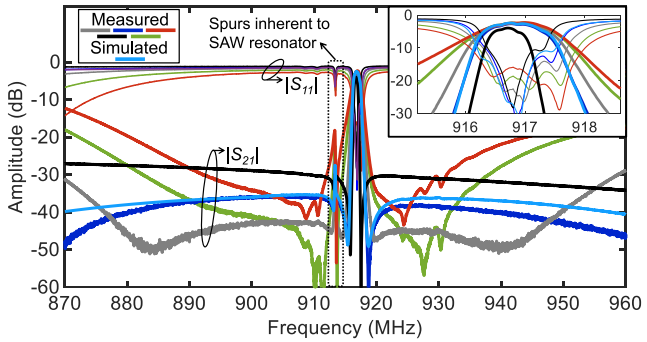

Fig. 11. RF-measured S-parameters of the four-stage quasi-elliptic AWLR BPF prototype with continuously tunable FBW. An EM-simulated state is also included for comparison purposes.

TABLE I
TRANSFER-FUNCTION-RECONFIGURABLE AWR BASED FILTERS

Ref.	Technology	Rec. modes	FBW(xk_t^2)	f_{cen}(MHz)
T.W	AWLR/SAW	E. Tun. BW	0.573-1.32	916.6
[19]	AWLR/SAW	M. Tun. BW	0.50-1.50	418
[12]	Ladder FBAR	S. BW BP/AS	0.33-0.50	2000
[13]	AWLR/FBAR	BP/AS	0.333	2130
[13]	AWLR/FBAR	BS/AP	0.31	2043
[22]	Ladder/ lattice FBAR	BP/AS	0.50	2000

(E. Tun.: electronically tunable, M. Tun.: manually tunable, S.: switchable, BP: bandpass, AP: all-pass, AS: all-stop, BS: bandstop)

the prototype is obtained by altering the DC biasing on the varactor diodes between (0 - 30 V). It can be observed that continuous BW tuning is obtained between 0.63–1.32 MHz (i.e., FBW=0.573 - $1.32k_t^2$) which corresponds to a tuning ratio (TR) of 2.31:1. For all tuning stages, the minimum IL was measured between 3.9-2.2 dB (effective Q (Q_{eff}) = 7700 - 6000) and the out-of-band IS levels were between 55-27 dB. An EM simulated state is also provided and appears to be in a good agreement successfully verifying the proposed filter concept. A comparison of the proposed multi-stage AWLR concept with state-of-the-art AWR-based reconfigurable filters is listed in Table I. As shown, this brief is the only one that allows electronically continuous BW tuning with enhanced FBW while exhibiting high Q_{eff}. The BPF concepts in [13], [22] only allow for reconfigurable transfer function states and the BPF in [12] facilitates discrete BW tuning. Lastly, the AWLR BPF concept in [19] is based on mechanically-tunable capacitors.

IV. CONCLUSION

This brief reported a new class of highly-selective quasi-elliptic BPFs that are based on cascaded multi-resonant stages of AWLRs. They exhibit enhanced FBW (>0.4-0.8k_t^2) that is continuously tunable by means of electronically-reconfigurable varactors. The concept can be readily scaled to higher-order transfer functions by cascading multi-resonant stages through impedance inverters. The multi-stage AWLR concept has been validated experimentally through a four-stage prototype at 916.6 MHz that shows tunable FBW between 0.57-1.32k_t^2, IL between 3.9-2.3 dB (Q_{eff} = 7700-6000), and out-of-band isolation levels > 27dB.

REFERENCES

[1] W. J. Chappell, E. J. Naglich, C. Maxey, and A. C. Guyette, "Putting the radio in 'software-defined radio': Hardware developments for adaptable RF systems," *Proc. IEEE*, vol. 102, no. 3, pp. 307–320, Mar. 2014.
[2] Y. I. Al-Yasir, N. O. Parchin, R. A. Abd-Alhameed, A. M. Abdulkhaleq, and J. M. Noras, "Recent progress in the design of 4G/5G reconfigurable filters," *Electronics*, vol. 8, no. 1, p. 114, Jan. 2019.
[3] M. Tian, Z. Long, L. Feng, L. He, and T. Zhang, "A compact wide-range frequency and bandwidth reconfigurable filter," *IEEE Microw. Wireless Compon. Lett.*, vol. 32, no. 11, pp. 1283–1286, Nov. 2022.
[4] R. Gómez-García, J.-M. Muñoz-Ferreras, J. Jimenéz-Campillo, F. Branca-Roncati, and P. Martín-Iglesias, "High-order planar bandpass filters with electronically-reconfigurable passband width and flatness based on adaptive multi-resonator cascades," *IEEE Access*, vol. 7, pp. 11010–11019, 2019.
[5] K. Zhao and B. D. Psychogiou, "Monolithically-integrated 3D printed coaxial bandpass filters and RF diplexers: Single-band and dual-band," *Int. J. Microw. Wireless Technol.*, vol. 14, pp. 1–11, Apr. 2022.
[6] T.-H. Lee, J.-J. Laurin, and K. Wu, "Reconfigurable filter for bandpass-to-absorptive bandstop responses," *IEEE Access*, vol. 8, pp. 6484–6495, 2020.
[7] S. Gong and G. Piazza, "Design and analysis of lithium–niobate-based high electromechanical coupling RF-MEMS resonators for wideband filtering," *IEEE Trans. Microw. Theory Techn.*, vol. 61, no. 1, pp. 403–414, Jan. 2013.
[8] A. Ding et al., "Enhanced electromechanical coupling in SAW resonators based on sputtered non-polar Al0.77Sc0.23N 1120 thin films," *Appl. Phys. Lett.*, vol. 116, no. 10, Mar. 2020, Art. no. 101903.
[9] Z. Hao et al., "Single crystalline ScAlN surface acoustic wave resonators with large figure of merit ($Q\times k_t^2$)," in *IEEE MTT-S Int. Microw. Symp. Dig.*, Boston, MA, USA, Jun. 2019, pp. 786–789.
[10] R. Su et al., "Wideband and low-loss surface acoustic wave filter based on 15° YX-$LiNbO_3$/SiO_2/Si structure," *IEEE Electron Device Lett.*, vol. 42, no. 3, pp. 438–441, Mar. 2021.
[11] H. Xu et al., "Large-range spurious mode elimination for wideband SAW filters on LiNbO3/SiO2/Si platform by $LiNbO_3$ cut angle modulation," *IEEE Trans. Ultrason., Ferroelectr., Freq. Control*, vol. 69, no. 11, pp. 3117–3125, Nov. 2022.
[12] M. Z. Koohi, S. Nam, and A. Mortazawi, "Intrinsically switchable and bandwidth reconfigurable ferroelectric bulk acoustic wave filters," *IEEE Trans. Ultrason., Ferroelectr., Freq. Control*, vol. 67, no. 5, pp. 1025–1032, May 2020.
[13] S. Nam, D. Psychogiou, and A. Mortazawi, "Reconfigurable transfer function BST acoustic wave lumped element resonator filters," in *Proc. Eur. Microw. Conf.*, 2021, pp. 301–304.
[14] A. F. Azarnaminy, J. Jiang, and R. R. Mansour, "Switched dual-band SAW filter using vanadium oxide switches," in *IEEE MTT-S Int. Microw. Symp. Dig.*, Jun. 2021, pp. 677–680.
[15] H. Wu, Y. Wu, Z. Lai, W. Wang, and Q. Yang, "A hybrid film-bulk-acoustic-resonator/coupled-line/transmission-line high selectivity wide-band bandpass FBAR filter," *IEEE Trans. Microw. Theory Techn.*, vol. 68, no. 8, pp. 3389–3396, Aug. 2020.
[16] H. Wu, Y. Wu, Z. Lai, W. Wang, and Q. Yang, "A hybrid filter with extremely wide bandwidth and high selectivity using FBAR network," *IEEE Trans. Circuits Syst. II, Exp. Briefs*, vol. 69, no. 7, pp. 3164–3168, Jul. 2022.
[17] N. S. Luhrs, D. J. Simpson, and D. Psychogiou, "Multiband acoustic-wave-lumped-element resonator-based bandpass-to-bandstop filters," *IEEE Microw. Wireless Compon. Lett.*, vol. 29, no. 4, pp. 261–263, Apr. 2019.
[18] D. Psychogiou, "Reconfigurable all-pass-to-bandstop acoustic-wave-lumped-element resonator filters," *IEEE Microw. Wireless Compon. Lett.*, vol. 30, no. 8, pp. 745–748, Aug. 2020.
[19] D. Psychogiou, R. Gómez-García, and D. Peroulis, "Tunable acoustic-wave-lumped-element resonator (AWLR)-based bandpass filters," in *IEEE MTT-S Int. Microw. Symp. Dig.*, San Fransisco, CA, USA, May 2016, pp. 1–4.
[20] D. Psychogiou, R. Gómez-García, and D. Peroulis, "Single and multi-band acoustic-wave-lumped–element-resonator (AWLR) bandpass filters with reconfigurable transfer function," *IEEE Trans. Microw. Theory Techn.*, vol. 64, no. 12, pp. 4394–4404, Dec. 2016.
[21] J. D. Larson, III, P. D. Bradley, S. Wartenberg, and R. C. Ruby, "Modified Butterworth-Van Dyke circuit for FBAR resonators and automated measurement system," in *Proc. IEEE Ultrason. Symp.*, San Juan, PR, USA, Oct. 2000, pp. 863–868.
[22] M. Z. Koohi, W. Peng, and A. Mortazawi, "An intrinsically switchable balanced ferroelectric FBAR filter at 2 GHz," in *IEEE MTT-S Int. Microw. Symp. Dig.*, Aug. 2020, pp. 131–134.